

2011

An Integrated Thermal and Mechanical Investigation of Molten-Salt Thermocline Energy Storage

S. Flueckiger

Purdue University - Main Campus

Z. Yang

Purdue University - Main Campus

S V. Garimella

Purdue University, sureshg@purdue.edu

Follow this and additional works at: <http://docs.lib.purdue.edu/coolingpubs>

Flueckiger, S.; Yang, Z.; and Garimella, S V., "An Integrated Thermal and Mechanical Investigation of Molten-Salt Thermocline Energy Storage" (2011). *CTRC Research Publications*. Paper 150.

<http://dx.doi.org/10.1016/j.apenergy.2010.12.031>

This document has been made available through Purdue e-Pubs, a service of the Purdue University Libraries. Please contact epubs@purdue.edu for additional information.

1 **An Integrated Thermal and Mechanical Investigation of**
2 **Molten-Salt Thermocline Energy Storage***

3
4 Scott Flueckiger¹, Zhen Yang², and Suresh V. Garimella^{1**}

5
6 ¹School of Mechanical Engineering

7 Cooling Technologies Research Center, an NSF IUCRC

8 585 Purdue Mall, Purdue University

9 West Lafayette, IN 47907-2088 USA

10
11 ² Key Laboratory for Thermal Science and Power Engineering of Ministry of Education

12 Department of Thermal Engineering

13 Tsinghua University

14 Beijing 100084 China

15
16
* Submitted for publication in *Applied Energy*, July 2010, and in revised form, September 2010

** Author to whom correspondence should be addressed: (765) 494-5621, sureshg@purdue.edu

1 **Abstract**

2 Thermal ratcheting is a critical phenomenon associated with the cyclic operation of dual-
3 medium thermocline tanks in solar energy applications. Although thermal ratcheting poses a
4 serious impediment to thermocline operation, this failure mode in dual-medium thermocline
5 tanks is not yet well understood. To study the potential for the occurrence of ratcheting, a
6 comprehensive model of a thermocline tank that includes both the heterogeneous filler region as
7 well as the composite tank wall is formulated. The filler region consists of a rock bed with
8 interstitial molten salt, while the tank wall is composed of a steel shell with two layers of
9 insulation (firebrick and ceramic). The model accounts separately for the rock and molten salt
10 regions in view of their different thermal properties. Various heat loss conditions are applied at
11 the external tank surface to evaluate the effect of energy losses to the surroundings. Hoop
12 stresses, which are governed by the magnitude of temperature fluctuations, are determined
13 through both a detailed finite element analysis and simple strain relations. The two methods are
14 found to yield almost identical results. Temperature fluctuations are damped by heat losses to
15 the surroundings, leading to a reduction in hoop stresses with increased heat losses. Failure is
16 prevented when the peak hoop stress is less than the material yield strength of the steel shell. To
17 avoid ratcheting without incurring excessive energy loss, insulation between the steel shell and
18 the filler region should be maximized.

19

20 **Keywords:** Solar thermal energy, thermal energy storage, molten-salt thermocline, thermal
21 ratcheting

22

1 **1. Introduction**

2 Concentrated Solar Thermal (CST) power plants [1-6] have been identified as a
3 promising renewable option for the economical generation of electricity at a large scale. The use
4 of a molten-salt thermocline for thermal energy storage (TES) in a CST power plant is believed
5 to lead to a potential reduction in capital cost of 35% relative to a two-tank counterpart [7,8]. In
6 a molten-salt thermocline, a molten salt (e.g., HITEC or HITEC XL [9]) is used as the heat
7 transfer fluid (HTF) that transports thermal energy between the storage unit and the other
8 sections of the power system such as the collector field and the steam generator. Separation
9 between the hot and cold zones of the molten salt is maintained by a thin slice of the tank which
10 experiences a large temperature gradient, known as the thermocline or heat exchange region.
11 This region is naturally enabled by buoyancy forces and preserves stable thermal stratification of
12 the fluid in the tank. To reduce the inventory of relatively expensive molten salt in the storage
13 system, a low-cost filler material compatible with molten salts, such as quartzite rock [10], is
14 used to fill much of the volume in the thermocline tank and acts as the primary thermal storage
15 material. Thermoclines of this type are termed dual-media or multi-media storage systems. A
16 detailed experimental demonstration of a dual-media thermocline on a pilot scale (2.3 MWh) was
17 reported in [11].

18 Despite its advantage in terms of cost, stability of the filler material in the hot molten-salt
19 environment as well as thermomechanically induced ratcheting are important concerns that need
20 attention in the design and operation of dual-media thermoclines. The first of these concerns is
21 addressed by appropriate choice of compatible filler material such as quartzite rock and silica
22 sand for nitrate salts (HITEC and HITEC XL). The thermal ratcheting problem, on the other
23 hand, requires a comprehensive understanding of the combined thermal and mechanical
24 characteristics of the tank and is the focus of the present work.

1 Thermal ratcheting is an important design issue in multiple applications [12,13], but has
2 not been extensively studied for dual-media thermoclines, in which thermal ratcheting can occur
3 when the system undergoes cycles of successive charge and discharge processes. As the tank
4 heats up during the charge half-cycle, its internal volume increases and the filler particles settle
5 lower to fill the additional volume created by the thermal expansion; as the tank cools down
6 during the discharge half-cycle, however, the filler particles cannot be displaced upward due to
7 gravity, inter-particle friction and resistance from particle packing. This prevents the tank wall
8 from shrinking to its original dimensions, resulting in a build-up of mechanical stress in the tank
9 shell through repeated operational cycles. If the stress in the tank shell reaches the yield point,
10 plastic deformation occurs. Further cycling can then lead to structural failure of the tank.

11 The largest thermocline facility to be constructed to date was the 10 MWe tank integrated
12 into the Solar One pilot plant [14]. A central receiver plant with direct steam generation, the
13 Solar One thermocline was an indirect storage system with synthetic oil (Caloria HT-43) used as
14 the HTF. Due to insufficient heliostats for excess solar harvesting, use of the storage subsystem
15 was sporadic and primarily provided auxiliary steam generation. Under these conditions of use,
16 thermal ratcheting was determined not to be a potential failure mode as the thermal expansion of
17 the filler material exceeded that of the carbon steel wall. Stresses in the tank wall were
18 monitored with strain gages to verify this assessment, but did suffer from large uncertainty in the
19 strain measurements.

20 It should be noted that the potential for thermal ratcheting is intimately related to the heat
21 transfer, tank structure, and materials used in thermocline systems, and depends on the design
22 and operational characteristics. It is important that both thermal and mechanical considerations
23 be investigated to ensure the absence of a potential for ratcheting.

1 An integrated analysis of the thermal and mechanical behavior of thermocline tanks of
2 different wall structures under different heat transfer boundaries is conducted in the present
3 study. The molten-salt flow and heat transfer in the tank are simulated by a two-temperature
4 model to account for the different thermal properties of the filler material and the salt; heat
5 transfer in the tank shell is included and is coupled with the molten-salt flow in the tank. The
6 resulting thermomechanical stress used for the prediction of thermal ratcheting is analyzed using
7 both finite element analysis and simple analytical strain relations. With this modeling approach,
8 the potential for thermal ratcheting of a thermocline tank is investigated for various composite
9 tank wall thicknesses and surface boundary conditions.

10

11 **2. Numerical Modeling**

12

13 *2.1 Problem Description*

14

15 A schematic representation of a TES thermocline tank is provided in Fig. 1. The tank of
16 inner diameter d is filled with a porous bed of quartzite rock to a height h . A molten salt (HITEC
17 [15]) serves as the heat transfer fluid (HTF) and flows through the filler bed to exchange heat
18 with the quartzite filler. The density, viscosity, and thermal conductivity of the HITEC fluid are
19 defined by the following temperature-dependent functions [16] derived from experimental data
20 [15]:

$$21 \quad \rho_l(T) = 1938 - 0.732(T_l - 200) \quad (1)$$

$$22 \quad \mu(T) = \exp[-4.343 - 2.0143(\ln(T_l) - 5.011)] \quad (2)$$

$$23 \quad k_l(T) = -0.000653(T_l - 260) + 0.421 \quad (3)$$

24 The specific heat of HITEC is 1561.7 J/kg-K, while the density and specific heat of quartzite
25 rock are 2201 kg/m³ and 964 J/kg-K, respectively. The effective thermal conductivity of the

1 dual-media mixture is computed using the correlation proposed by Gonzo [17]. The porosity of
2 the filler region is assumed to be 0.22 with an average filler particle size of 0.05 m.

3 In this work, the tank dimensions d and h are set to be equal although there are many other
4 options for tall ($d < h$) and flat ($d > h$) thermocline systems. Above and below the porous filler
5 bed are distributors of height h' ($h' = 0.05h$), which are free of quartzite rock. These distributor
6 regions serve to maintain a uniform flow condition at both ends of the filler bed in order to
7 achieve good thermal stratification. The distributors are connected to the rest of the system with
8 tubes of diameter d' ($d' = 0.05d$) at the top and bottom ports.

9 During the charge half-cycle, a hot molten-salt flow at a high temperature level T_h from the
10 collector field is pumped through the top port into the tank, heating up and thus storing solar heat
11 in the filler particles; during the discharge half-cycle, a cold molten-salt flow at a lower
12 temperature level T_c is pumped through the bottom port into the tank, heated by the hot filler
13 particles and exhausted from the top port. Early in the discharge process, molten-salt outflow
14 through the top port is maintained at the desired high temperature level, and is delivered for
15 generating superheated steam for electricity production. As the discharge process continues, the
16 outflow decreases in temperature, eventually falling to a value that is no longer suitable for
17 generating steam. As a result, only a portion of the initially stored thermal energy can be
18 retrieved as useful heat.

19 The tank considered here has a complex wall consisting of multiple layers [18,19]: an inner
20 firebrick layer for thermal isolation, a steel shell layer for mechanical support and an outer layer
21 of ceramic fiber for corrosion protection and thermal insulation. To inhibit leakage of the molten
22 salt through the internal insulation, a thin liner material is installed between the rock and
23 insulation. The liner is corrugated to accommodate thermal expansion and contraction

1 associated with the operation of the thermocline. The length scale of these corrugations is
 2 assumed to be smaller than the size of the granular filler, inhibiting full contact with the rock and
 3 preventing crushing of the liner. Due to the small relative thickness of the corrugated liner, its
 4 thermal effects are neglected.

5 Relevant thermal transport properties for the two insulation materials and structural shell are
 6 listed in Table 1. The tank is built on a concrete foundation which is cooled by embedded water
 7 tubes; its side and top walls are exposed to atmosphere. Therefore, the thermal boundary
 8 conditions on the external wall of the tank are set to a mixed convection and radiation heat
 9 transfer condition on the exposed walls, and a constant temperature condition on the bottom wall.

10 2.2 Governing Equations

11 (a) Molten-salt flow and heat transfer inside thermocline tank

12 Mass and momentum transport of the molten salt in the fillerbed are governed by [16]:

$$13 \frac{\partial(\varepsilon\rho_l)}{\partial t} + \nabla \cdot (\rho_l \bar{u}) = 0 \quad (4)$$

$$14 \frac{\partial(\varepsilon\rho_l)}{\partial t} + \nabla \cdot \left(\rho_l \frac{\bar{u}\bar{u}}{\varepsilon} \right) = -\varepsilon \nabla \cdot p + \nabla \cdot \bar{\bar{\tau}} + \varepsilon \rho_l \bar{g} - \varepsilon \left(\frac{\mu}{K} \bar{u} + \frac{F}{\sqrt{K}} \rho_l |\bar{u}| \bar{u} \right) \quad (5)$$

15 The stress tensor is defined as $\bar{\bar{\tau}} = 2\mu\bar{\bar{S}} - \frac{2}{3}\mu S_{kk}\bar{\bar{I}}$, where $\bar{\bar{S}} = \frac{1}{2}(\nabla\bar{u} + (\nabla\bar{u})^T)$. The spatial
 16 gradient for polar coordinates is $\nabla = \bar{e}_r \frac{\partial}{\partial r} + \bar{e}_\theta \frac{1}{r} \frac{\partial}{\partial \theta} + \bar{e}_x \frac{\partial}{\partial x}$, although the axisymmetric
 17 assumption for the thermocline operation in this work eliminates any dependency in the
 18 circumferential direction (θ). In contrast to the fillerbed, molten-salt flow in the tank distributors
 19 is turbulent. To account for this local turbulence, the standard k- ε model is enforced in the
 20 distributor regions [20].

1 For the two-temperature model with co-located data storage, the energy transport
 2 equations for the molten salt (subscripted l) and the solid filler (subscripted s) provided below
 3 are coupled by the interstitial heat transfer. The interstitial heat transfer coefficient, h_i , is
 4 computed from the Nusselt number (Nu) associated with this inter-phase exchange which is
 5 obtained from the correlation of Wakao and Kagueli for forced convection inside a packed bed
 6 [21].

$$7 \quad \frac{\partial[\varepsilon\rho_l C_{p,l}(T_l - T_c)]}{\partial t} + \nabla \cdot [\rho_l \bar{u} C_{p,l}(T_l - T_c)] = \quad (6)$$

$$\nabla \cdot (k_e \nabla T_l) + p \nabla \cdot \bar{u} + tr \left[\nabla \left(\frac{\bar{u}}{\varepsilon} \right) \cdot \bar{\tau} \right] + \frac{\bar{u} \cdot \bar{u}}{2\varepsilon} \times \frac{\partial \rho_l}{\partial t} + h_i (T_s - T_l)$$

$$8 \quad \frac{\partial}{\partial t} [(1 - \varepsilon) \rho_s C_{p,s} (T_s - T_c)] = -h_i (T_s - T_l) \quad (7)$$

9 Each of the governing transport equations can be readily non-dimensionalized, as
 10 presented in the literature [16,22].

11 (b) Boundary conditions

12 During discharge of the thermocline tank, molten salt enters the bottom distributor at a
 13 fixed velocity and temperature:

$$14 \quad \bar{u} = \left(\frac{d}{d'} \right)^2 u_m \bar{e}_x, \quad T = T_c \quad (8)$$

15 At the outflow from the upper thermocline distributor:

$$16 \quad \frac{\partial \bar{u}}{\partial x} = 0, \quad \frac{\partial T}{\partial x} = 0 \quad (9)$$

17 Due to the elevated temperatures of the molten salt, the ceramic exterior of the
 18 thermocline tank experiences heat exchange with the surroundings by both convection and
 19 radiation:

$$\left. \frac{\partial T_3}{\partial r} \right|_w = -\frac{h_w}{k_3} (T_w - T_\infty) - \frac{\varepsilon_w \sigma_r}{k_3} (T_w^4 - T_\infty^4) \quad (10)$$

(c) Heat conduction in composite wall

While convection and radiation occur at the tank surface, heat is transported by conduction in each layer of the composite wall according to the heat diffusion equation with properties inserted appropriately for each layer:

$$\rho C_p \frac{\partial T}{\partial t} = -k \nabla \cdot T \quad (11)$$

To account for heat transfer at the two solid interfaces (firebrick and steel, steel and ceramic), the following heat balance is applied:

$$\left. \frac{\partial T_1}{\partial r} \right|_{12} = \frac{k_2}{k_1} \left. \frac{\partial T_2}{\partial r} \right|_{12}, \quad \left. \frac{\partial T_2}{\partial r} \right|_{23} = \frac{k_3}{k_2} \left. \frac{\partial T_3}{\partial r} \right|_{23} \quad (12)$$

(d) Mechanical stress

All solid materials experience some finite change in volume when exposed to an increase in temperature. The steel tank shell can expand or contract freely in the height direction as no structural restrictions are applied in this direction; *in the circumferential direction, however, deformation is determined by the maximum temperature experienced at each axial location and then holds constant (as explained below) provided the yield stress of the material has not been exceeded.* The possibility of thermal ratcheting (which occurs upon plastic deformation of the shell) must thus be investigated only in the circumferential direction, henceforth referred to as the principal direction. In the principal direction, the amount of change or strain is composed of two parts: thermal strain ε_T and mechanical strain ε_M , represented as:

$$\varepsilon_L(x, r) = \varepsilon_T + \varepsilon_M \quad (13)$$

1 The thermal strain is dependent on the coefficient of thermal expansion (α_L) for the given
2 material:

$$3 \quad \varepsilon_T(x, r) = \alpha_L [T_2(x, r) - T_{ref}] \quad (14)$$

4 The mechanical strain is related to the modulus of elasticity (E) of the steel and the principal
5 stress (σ):

$$6 \quad \varepsilon_M(x, r) = \frac{\sigma}{E} \quad (15)$$

7 The weight of the filler bed and molten salt in the tank exerts pressure on the tank wall, inducing
8 a certain amount of mechanical stress in the steel tank shell. However this stress ($\sim 10^5$ Pa) is
9 negligible compared to that caused by tank contraction ($\sim 10^7$ - 10^8 Pa).

10 When the steel tank wall is heated to its maximum temperature in a charge half-cycle, the
11 thermal strain also reaches its maximum. Since the filler region does not prevent expansion and
12 the tank wall can expand freely, the mechanical strain ε_M remains at zero, resulting in the total
13 strain of the tank being solely that due to thermal strain, as shown in Eq. (13). Strain interaction
14 with the firebrick and ceramic sections is neglected as these layers are composed of loosely
15 connected blocks, and are therefore unable to provide structural support to the filler region. In
16 any case, if the filler imposes an unacceptable level of stress on the firebrick, an alternative
17 insulation material may be substituted with similar thermal properties, such as thermal wool.
18 The term “firebrick” is used here in a generic sense, and does not refer to a specific material.

19 While the filler medium settles into the expanded volume, it cannot be dislodged upward
20 to allow contraction of the tank wall to its original shape when cooled by cold molten salt flow in
21 the discharge half-cycle. Therefore, the steel tank wall is ratcheted at the geometry it reached at
22 the maximum temperature; in other words, the strain ε_L in Eq. (13) is fixed at its maximum value.

1 When the steel tank subsequently cools in a discharge half-cycle, the thermal strain is reduced,
2 resulting in an increase in the mechanical strain. The mechanical strain is maximized when the
3 steel reaches its minimum temperature, i.e., ε_T reaches its minimum value in a cycle. For
4 operational safety, this maximum mechanical stress σ_{\max} must not exceed the tensile stress of the
5 tank steel σ_y :

$$6 \quad \sigma_{\max}(x, r) = \alpha_L E [T_{2,\max}(x, r) - T_{2,\min}(x, r)] < \sigma_y \quad (16)$$

7 Equation (16) can be rewritten as

$$8 \quad F_s \cdot \Delta T = \frac{\sigma_y}{\alpha_L \cdot E} \quad (17)$$

9 where F_s is the factor of safety. Equation (17) provides a design criterion for any potential tank
10 material. For simplicity of calculation, both the expansion coefficient and the modulus of
11 elasticity are assumed to be independent of temperature.

12 Based on this criterion, the factor of safety F_s associated with thermal ratcheting is
13 maximized by the implementation of highly resilient materials for the steel shell as well as
14 insulation to isolate the shell from the molten-salt temperature fluctuations, provided in the
15 current design by the firebrick. For mechanical analysis of the steel, the coefficient of thermal
16 expansion, modulus of elasticity, and yield strength are assumed to take typical values of
17 0.00001 K^{-1} , 200 GPa, and 200 MPa, respectively.

18 *2.3 Solution Procedure*

19 Governing equations for the thermal analysis are solved using the commercial
20 computational fluid dynamics (CFD) software, FLUENT 12.1.4 [23]. The thermocline tank and
21 wall domains are discretized into 15750 cells for this finite-volume computation. Spatial
22 discretization of the convective fluxes is performed with a second-order upwind scheme.

1 Transient discretization is performed with a first-order implicit formulation with a non-
2 dimensional time step of $\Delta\tau = 0.0004$. Time step-independence is verified by comparing results
3 with a reduced non-dimensional time step of $\Delta\tau = 0.0001$. The PISO algorithm is applied for
4 pressure-velocity coupling [24]. A converged solution is considered to have been achieved at
5 each time step when all dimensionless residuals reduce to less than 10^{-4} .

6 At the start of the simulation, the entire thermocline tank domain is initialized to the hot
7 limit of the molten salt discharge (T_h). In an adiabatic model, this would be a valid initialization
8 as all energy lost through the discharge is recouped in the subsequent charge process. However,
9 since convection and radiation are included at the exposed tank surfaces in the present work, an
10 isothermal condition is not realized at the start of each cycle. Multiple discharge and charge
11 half-cycles are therefore simulated in succession until a periodic response develops in the entire
12 domain.

13 Once periodicity is achieved in the domain, the vertical temperature distribution in the
14 steel shell is extracted at multiple times throughout the discharge and charge processes. The
15 maximum and minimum temperatures at each discretized location along the wall are extracted
16 from these instantaneous profiles. These limiting temperatures are then organized into profiles
17 that represent the maximum and minimum values experienced at each location during one
18 complete cycle. The maximum temperature profile determines the final shape and relative
19 position of the tank wall as a result of thermal expansion. Based on this new wall geometry, the
20 minimum temperature profile determines the maximum amount of hoop stress that develops due
21 to the inability of the wall to contract around the reoriented filler region after the settling process.

22 To solve for the hoop stress, the steel layer is discretized into several deformable solid 2-
23 dimensional elements with the commercial finite element analysis software, ANSYS 12.1 [25].

1 The non-dimensional size of these elements is $\Delta X = 0.00173$. Temperatures from the maximum
2 profile identified above are applied along the wall to solve for the resultant radial deflections.
3 These deflections are small and assumed to be decoupled from the internal molten-salt behavior.
4 The radial deflections are then fixed while temperatures from the minimum profile are reapplied
5 along the wall to solve for the hoop stress. An alternative approach is to solve for the stress
6 directly from the localized temperature fluctuations with Eq. 16. This second approach is less
7 computationally intensive, but assumes that the remaining principal and shear stresses in the steel
8 shell are negligible relative to the hoop stress.

9 The fluid flow and heat transfer model was verified against the experimental results from
10 a pilot-scale TES thermocline (2.3MWh) [11] with good agreement [16]. While results from the
11 mechanical analysis could not be validated against experiments due to the absence of reliable
12 data in the literature, the use of two independent approaches – analytical and finite-element –
13 provides a verification.

14

15 **3. Results and discussion**

16 To investigate tank behavior for various surface conditions and composite wall
17 thicknesses, seven different thermocline tank cases were considered. The composite wall
18 characteristics for each case are summarized in Table 2. In each case, the height and diameter of
19 the filler bed region were both fixed at 12 m to maintain similarity with respect to tank operation.
20 The hot and cold operation limits of the molten salt were also fixed at 450 °C and 293 °C,
21 respectively. The temperature of the surroundings is fixed at 27 °C. In cases 1 through 4, the
22 tank wall configurations were held constant while the convection coefficient was varied between
23 5 and 10 W/m²-K and the surface emissivity was varied between 0.5 and 1. In cases 5 through 7,

1 the surface parameters were held constant while the individual thicknesses of the composite wall
2 layers were varied. To account for water cooling at the tank foundation, the bottom wall surface
3 temperature was set at 90 °C in all cases.

4 As previously discussed, each case required a minimum of five full (discharge and
5 charge) cycles to achieve thermally periodic behavior. Both the discharge and charge processes
6 were computed for six hours of flow time. An additional cycle was required for simulation of
7 case 5 due to the increased thickness of the firebrick layer. Temperature data were extracted
8 from the final discharge and charge processes.

9 *3.1 Flow and temperature fields*

10 Temperature results for case 1 (listed in Table 1) are plotted in Fig. 2 at three separate
11 times during the discharge process. In view of the assumption of axial symmetry, only half of
12 the vertical cross-section view is provided. Early in the discharge ($\tau = 0.513$), only molten salt at
13 the hot temperature limit is present in the upper half of the thermocline. This zone diminishes
14 with time as hot salt is extracted and the thermocline region travels up the filler region. At the
15 end of the six-hour discharge process ($\tau = 6.516$), the high-temperature salt supply is exhausted
16 and salt is available at progressively cooler temperatures.

17 It can also be seen from the temperature distributions in the figure that the composite wall
18 region is cooler than the molten salt due to direct exposure to surface convection and radiation.
19 To better illustrate the temperature distribution in the wall, the time-dependent thermal response
20 of the steel shell is plotted in Fig. 3. Temperature profiles at non-dimensional times greater than
21 6.156 occur during the subsequent charge half-cycle, and are included to reflect the periodic
22 reheating response of the steel wall. The presence of a phase shift between the wall temperature
23 response and the tank operation is expected due to the inherent thermal mass of the composite

1 wall. Throughout the complete tank operating cycle, the steel wall temperatures remain below
2 the temperature operation limits of the molten salt. Within this smaller temperature range, the
3 temperature variation with time is at a maximum near the center tank height due to the presence
4 of the thermocline region. Near the distributors, this variation is minimal as the traversal of the
5 thermocline region does not extend to the upper and lower extremes of the fillerbed.

6 While the composite wall is cooled directly due to external losses, molten salt close to the
7 wall is also cooled. As a result, reversed flow of the cooled molten salt can occur along the wall
8 due to buoyancy forces, since the tank discharge velocity in the filler bed is quite low.
9 Occasional swirling and overall disruption of flow uniformity can thus be caused in the filler
10 region despite the inlet flow from the distributor being uniform. As seen in Fig. 2, these effects
11 are most prominent far from the thermocline region where molten-salt temperature gradients are
12 minimal. Early in the discharge, swirling occurs closer to the wall in the large high-temperature
13 region at the top of the fillerbed. This swirling decays with discharge time as the local
14 temperature gradients are eventually dominated by the moving thermocline region. However, a
15 simultaneous growth of the cold-temperature region occurs at the fillerbed bottom and ultimately
16 results in a new swirl pattern later in the discharge process.

17 *3.2 Outflow Temperature History*

18 In each of the seven cases, the cooling effect from external losses is limited to regions
19 near the tank wall. Thus the discharge performance did not vary to a large extent from case to
20 case. This trend is illustrated in Fig. 4 which shows the average salt temperatures at the
21 discharge port over all cases as a function of time. The discharge temperature variation among
22 the cases is represented by the error bars equal to twice the standard deviation of the sample (s),
23 where s is defined as:

$$s = \sqrt{\frac{1}{N} \sum_{i=1}^N (T_i - \bar{T})^2} \quad (18)$$

Though the spread in temperature between the cases increases with discharge time, the salt temperatures remain relatively clustered, with the maximum temperature difference between the seven cases being less than 7% of the total molten-salt operation range at the end of the discharge half-cycle.

In all cases, high temperature molten-salt outflow is maintained early in the discharge process. Halfway through the discharge, a rapid decline in temperature occurs with an eventual drop to nearly 50% of the molten-salt operation range. The viability of this colder discharge for steam generation depends on the flexibility of the applied Rankine cycle, such as through the use of sliding-pressure operation [26]. In view of the relative insensitivity of the thermocline behavior to details of the tank wall and the heat losses, the recommended approach to prolonging the high-temperature discharge period is to increase the filler region volume.

3.3 Tank Wall Stress

Temperature data from the steel tank shell was extracted from the computed temperature field during the discharge process for stress analysis. As previously discussed, hoop stress may be determined with two separate approaches: (1) by performing an FEA simulation of the steel layer, or (2) by solving for stress directly from the CFD temperature data with Eq. 16. Results from the two approaches applied to the wall temperature data from case 1 are plotted in Fig. 5 for comparison. In the plot, hoop stress is normalized with respect to the yield strength as follows:

$$\omega = \frac{1}{F_s} = \frac{\sigma}{\sigma_y} \quad (19)$$

1 The two approaches are seen to yield almost identical results. Due to its simplicity, the second
2 approach was adopted for computing the hoop stress for the remaining cases. The normalized
3 results for all seven cases are plotted in Fig. 6.

4 In cases 1 through 4, the maximum hoop stress is inversely proportional to the heat loss
5 at the tank surface. Among these cases, case 2 experiences the greatest external heat transfer and
6 generates the lowest peak stress value. In contrast, case 3 experiences the least amount of
7 external heat transfer but generates the highest peak stress value. This behavior is due to the
8 sensitivity of the temperature distribution in the composite wall to both external losses and cyclic
9 tank operation. Greater losses at the surface reduce sensitivity to the molten salt fluctuations and
10 dampen cyclic temperature variations along the steel shell. It is also noted that all cases yield
11 normalized peak stress values less than one, with cases 1 through 4 clustered between 0.407 and
12 0.424. Thus plastic deformation-associated ratcheting would not occur in any of these cases.
13 Since thermal ratcheting is not an issue, case 3 may provide the optimum scenario due to the
14 minimal energy losses to the surroundings.

15 Even though the tank wall does not reach very high stress levels in cases 1 to 4, further
16 reductions in stress can maximize the factor of safety associated with thermal ratcheting in the
17 event of unexpected increases in heat loss or other unforeseen circumstances. The structure of
18 the composite wall is modified in cases 5 to 7 in terms of the relative thicknesses of the firebrick,
19 steel shell, and ceramic exterior layers, while the surface heat loss conditions are held at the
20 values in case 1. Case 5 experiences the lowest overall peak stress in the steel shell with a
21 normalized value of 0.129 due to the increased firebrick thickness. The added insulation
22 between the filler region and the steel in this case diminishes sensitivity to the fluctuating
23 molten-salt temperatures. Case 6 also exhibits much lower stress levels, with a normalized value

1 of 0.333. The thicker steel layer in this case increases axial conduction which reduces
2 temperature gradients along the shell.

3 In contrast to the behavior of the firebrick and steel layers, the external ceramic layer
4 thickness must be reduced to decrease hoop stress in the steel shell. A thinner ceramic layer
5 increases the sensitivity of the steel shell to the external losses, which in turn decreases
6 sensitivity to the cyclic molten-salt behavior and dampens temperature fluctuations. This effect
7 is seen in case 7, where the ceramic-layer thickness is reduced by a factor of two compared to the
8 other cases to yield a peak normalized hoop stress of 0.391. However since the peak stress is
9 only reduced by 5% compared to case 1, a larger ceramic layer remains preferable to maximize
10 total insulation between the filler region and the surroundings.

11

12 **4. Conclusions**

13

14 A comprehensive thermal model of a molten-salt thermocline tank with a composite wall
15 structure is used to investigate the potential for failure of the tank shell wall by thermal
16 ratcheting. While hoop stress associated with thermal ratcheting can be resolved with a finite
17 element simulation of the steel shell, nearly identical results can be obtained through simpler
18 analytical strain relations. Various non-adiabatic surface conditions and composite wall
19 geometries are evaluated for their effects on ratcheting potential. The inclusion of external
20 losses at the tank surface affects the flow field in the filler region with reversed flow and swirl
21 patterns being induced in the filler bed during discharge. However, these effects are
22 concentrated near the wall, and do not greatly alter the overall discharge performance.

23 Hoop stress in the steel shell is a direct consequence of temperature changes generated by
24 the cyclic operation of the thermocline unit. The effects of these cyclic changes on the stresses

1 induced in the steel tank wall are successfully damped by increasing either the surface heat
2 losses or the insulation between the filler region and the steel wall. As surface losses are
3 detrimental to energy storage in the thermocline tank, the recommended solution is to maximize
4 the internal insulation to minimize the potential for thermal ratcheting. Tank wall stresses can
5 also be alleviated by increasing the steel shell thickness to improve axial conduction, but this
6 may lead to impractical tank aspect ratios or excessive radial temperature gradients within the
7 steel.

8

1 Nomenclature

2	C_p	specific heat, $J\ kg^{-1}\ K^{-1}$
3	d	diameter of thermocline tank, m
4	d'	diameter of inlet and outlet ports, m
5	d_s	diameter of filler particles, m
6	E	modulus of elasticity, GPa
7	\bar{e}	unit vector, -
8	F	inertial coefficient, $F = \frac{1.75}{\sqrt{150\varepsilon^3}}$ [27], -
9	F_s	factor of safety, -
10	g	acceleration due to gravity, m/s^2
11	h	height of thermocline tank, m
12	h'	height of distributor region, m
13	h_i	interstitial heat transfer coefficient, $W\ m^{-2}\ K^{-1}$
14	K	permeability, $K = \frac{d_s^2 \varepsilon^3}{175(1-\varepsilon)^2}$ [28], m^2
15	k	thermal conductivity, $W\ m^{-1}\ K^{-1}$
16	p	pressure, Pa
17	R	non-dimensional tank radius, -
18	T	temperature, K
19	t	time, s
20	\bar{u}	velocity vector, m/s
21	u_m	mean velocity magnitude at inlet to filler region, m/s
22	X	non-dimensional tank height, $X = x/h$, -

1 **Greek**

2 α thermal diffusivity, m^2/s

3 α_L coefficient of thermal expansion, K^{-1}

4 δ composite wall layer thickness, m

5 ε porosity, -

6 ε_L strain, -

7 ε_r emissivity, -

8 μ viscosity, Pa s

9 Θ non-dimensional temperature, $\Theta = \frac{T-T_c}{T_h-T_c}$, -

10 θ polar angle, rad

11 ρ density, kg/m^3

12 τ non-dimensional time, $\tau = t \cdot u_m / h$, -

13 σ stress, Pa

14 σ_r Stefan-Boltzmann constant, $5.67 \times 10^{-8} \text{ W m}^{-2} \text{ K}^{-4}$

15 ω stress ratio, -

16 **Subscript**

17 1 firebrick

18 2 steel

19 3 ceramic

20 c cold operation limit

21 h hot operation limit

22 l liquid salt phase

23 max maximum

1	min	minimum
2	r	radial direction
3	ref	reference
4	s	solid filler phase
5	w	exterior tank surface
6	x	x direction
7	y	yield strength
8	θ	circumferential direction

9

10 **References**

- 11 1. Klaiß H, Köhne R, Nitsch J, Sprengel U, Solar thermal power plants for solar countries –
12 technology, economics, and market potential, *Appl Energy* 1995;52:165-83.
- 13 2. Ravi Kumar K, Reddy KS, Thermal analysis of solar parabolic trough with porous disc
14 receiver, *Appl Energy* 2009; 86:1804-12.
- 15 3. Wu SY, Xiao L, Cao Y, Li YR, A parabolic dish/AMTEC solar thermal power system
16 and its performance evaluation, *Appl Energy* 2010;87:452-62.
- 17 4. Cavallero F, Fuzzy TOPSIS approach for assessing thermal-energy storage in
18 concentrated solar power (CSP) systems, *Appl Energy* 2010;87:496-503.
- 19 5. Yang M, Yang X, Yang X, Ding J, Heat transfer enhancement performance of the molten
20 salt receiver of a solar power tower, *Appl Energy* 2010;87:2808-11.
- 21 6. Kolb G, Hassani V, Performance analysis of thermocline energy storage proposed for the
22 1 MW Saguaro solar trough plant, *Proc of ISEC 2006; Denver, CO.*

- 1 7. Price H, A parabolic trough solar power plant simulation model, Proc of ISES 2003;
2 Hawaii Island, HI.
- 3 8. Kearney and Associates, Engineering evaluation of a molten salt HTF in a parabolic
4 through solar field, NREL Contract No. NAA-1-30441-04; 2001,
5 http://www.nrel.gov/csp/troughnet/pdfs/ulf_herrmann_salt.pdf, as accessed July 2010.
- 6 9. Kearney D, Herrmann U, Nava P *et al.*, Assessment of a molten salt heat transfer fluid in
7 a parabolic through solar field, J Sol Energy Eng 2003;125:170-6.
- 8 10. Brosseau D, Kelton JW, Ray D, Edgar M, Testing of thermocline filler materials and
9 molten-salt heat transfer fluids for thermal energy storage systems in parabolic trough
10 power plants, J Sol Energy Eng 2005;127:109-16.
- 11 11. Pacheco JE, Showalter SK, Kolb WJ, Development of a molten-salt thermocline thermal
12 storage system for parabolic trough plants, J Sol Energy Eng 2002;124:153-9.
- 13 12. Igari T, Wada H, Ueta M, Mechanism-based evaluation of thermal ratcheting due to
14 traveling temperature distribution, ASME J Pressure Vessel Technol 2000;122:130-8.
- 15 13. Russell-Stevens M, Todd RI, Papakyriacou M, Thermal expansion behaviour of ultra-
16 high modulus carbon fibre reinforced magnesium composite during thermal cycling, J
17 Mater Sci 2006;41:6228-36.
- 18 14. Faas SE, Thorne LR, Fuchs EA, Gilbersten ND, 10 MWe solar thermal central receiver
19 pilot plant: thermal storage subsystem evaluation – final report, Sandia National
20 Laboratories SAND86-8212; 1986.
- 21 15. HITEC heat transfer salt, Coastal Chemical Co., LLC, Brenntag Company,
22 <http://www.coastalchem.com/>, as accessed July 2010.

- 1 16. Yang Z, Garimella SV, Thermal analysis of solar thermal energy storage in a molten-salt
2 thermocline, Sol Energy 2010;84:974-85.
- 3 17. Gonzo EE, Estimating correlations for the effective thermal conductivity of granular
4 materials, J Chem Eng 2002;90:299-302.
- 5 18. Kolb GJ, Nikolai U, Performance evaluation of molten salt thermal storage systems,
6 Sandia National Laboratories SAND87-3002; 1988.
- 7 19. Gabbrielli R, Zamparelli C, Optimal design of a molten salt thermal storage tank for
8 parabolic trough solar power plants, J Sol Energy Eng 2009;131:041001-10.
- 9 20. Launder BE, Spalding DB, Lectures in mathematical models of turbulence. London,
10 England: Academic Press; 1972.
- 11 21. Wakao N, Kaguei S, Heat and mass transfer in packed beds. New York: Gordon and
12 Beach; 1982.
- 13 22. Yang Z, Garimella SV, Molten-salt thermal energy storage in thermocline under different
14 environmental boundary conditions, Appl Energy, 2010;873322-3329.
- 15 23. FLUENT 12.1.4 Documentation, Fluent Inc., as accessed July 2010.
- 16 24. Issa RI, Solution of implicitly discretized fluid flow equations by operator splitting, J
17 Comput Phys 1986;62:40-65.
- 18 25. ANSYS 12.1 Documentation, ANSYS Inc., as accessed July 2010.
- 19 26. Solar Thermocline Storage Systems: Preliminary Design Study. EPRI, Palo Alto, CA:
20 2010. 1019581.
- 21 27. Krishnan S, Murthy JY, Garimella SV, A two-temperature model for analysis of passive
22 thermal control systems, J Heat Transfer 2004;126:628-37.

1 28. Beckermann C, Viskanta R, Natural convection solid/liquid phase change in porous
2 media, Int J Heat Mass Transfer 1988;31:35-46.

3
4

1
2

3
4

Table 1. Thermal transport properties of composite wall layers.

Material	k (W/m-K)	ρ (kg/m³)	C_P (J/kg-K)
Firebrick	1	2000	1000
Steel	60	8000	430
Ceramic	1	1000	1000

1 Table 2. Summary of the cases considered with different wall structural parameters and heat loss
2 conditions.
3

Case	h (W/m ² -K)	ϵ_r	δ_{fb} (m)	δ_{cs} (m)	δ_{cer} (m)
1	5	1	0.1	0.02	0.05
2	10	1	0.1	0.02	0.05
3	5	0.5	0.1	0.02	0.05
4	10	0.5	0.1	0.02	0.05
5	5	1	0.2	0.02	0.05
6	5	1	0.1	0.04	0.05
7	5	1	0.1	0.02	0.025

4
5
6

1 **Figure Captions**

2

3 Figure 1. Schematic illustration of the thermocline tank with a composite wall consisting of

4 firebrick (1), steel (2), and ceramic (3).

5 Figure 2. Normalized temperature and flow fields of the case 1 thermocline tank at early (τ

6 $= 0.513$), midpoint ($\tau = 3.078$), and end ($\tau = 6.156$) stages of the discharge

7 process.

8 Figure 3. Temperature profiles along the steel shell (case 1).

9 Figure 4. Molten-salt outflow temperature during thermocline tank discharge (averaged

10 over all cases). Variation between the cases is represented with error bars equal

11 to two standard deviations (Eq. 18).

12 Figure 5. Comparison of hoop stresses determined for case 1 using finite element analysis

13 (FEA) and analytical strain relations.

14 Figure 6. Hoop stress profiles along the fillerbed height for all cases (see Table 2).

Figure_1
[Click here to download high resolution image](#)

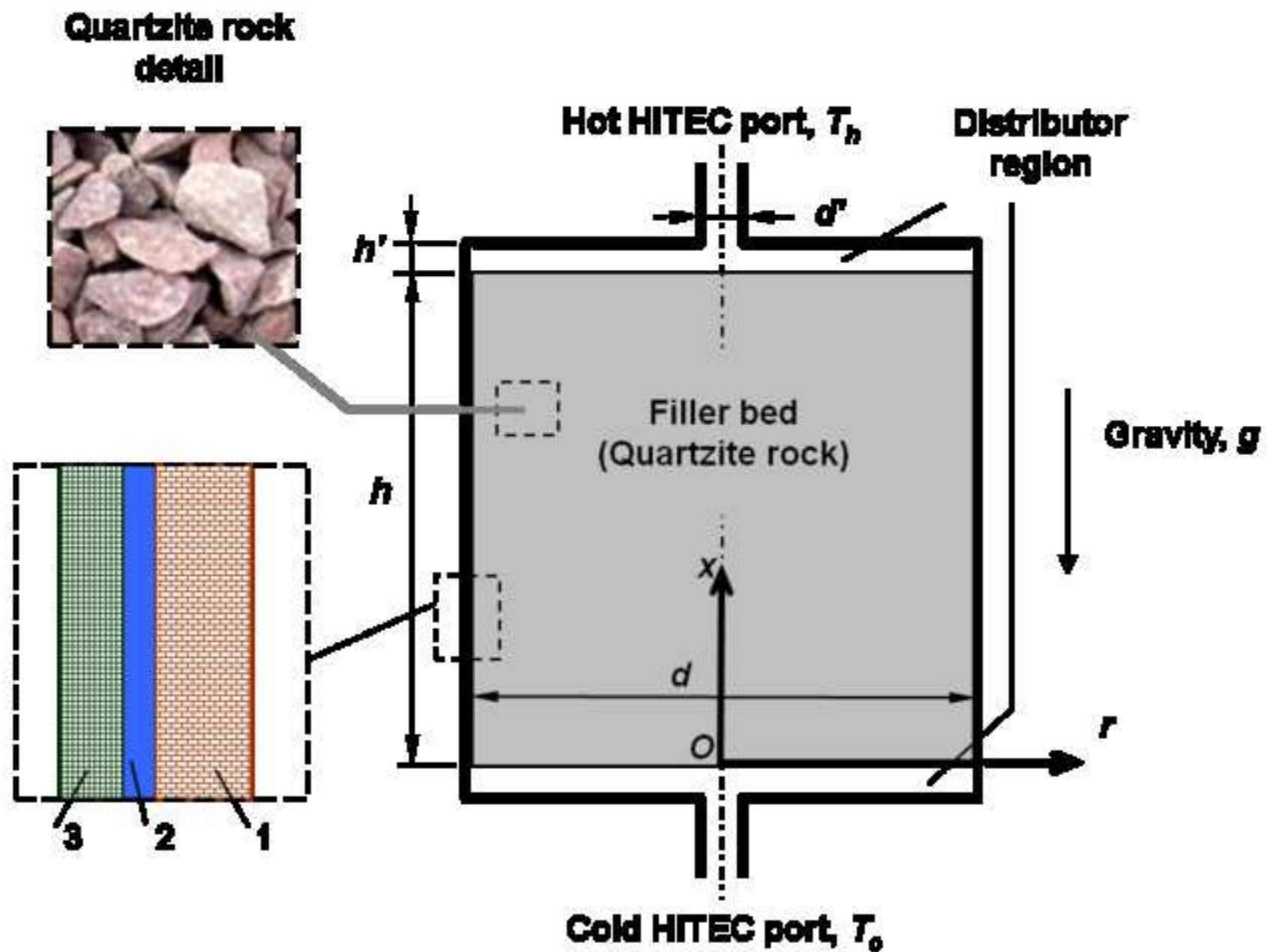


Figure_2
[Click here to download high resolution image](#)

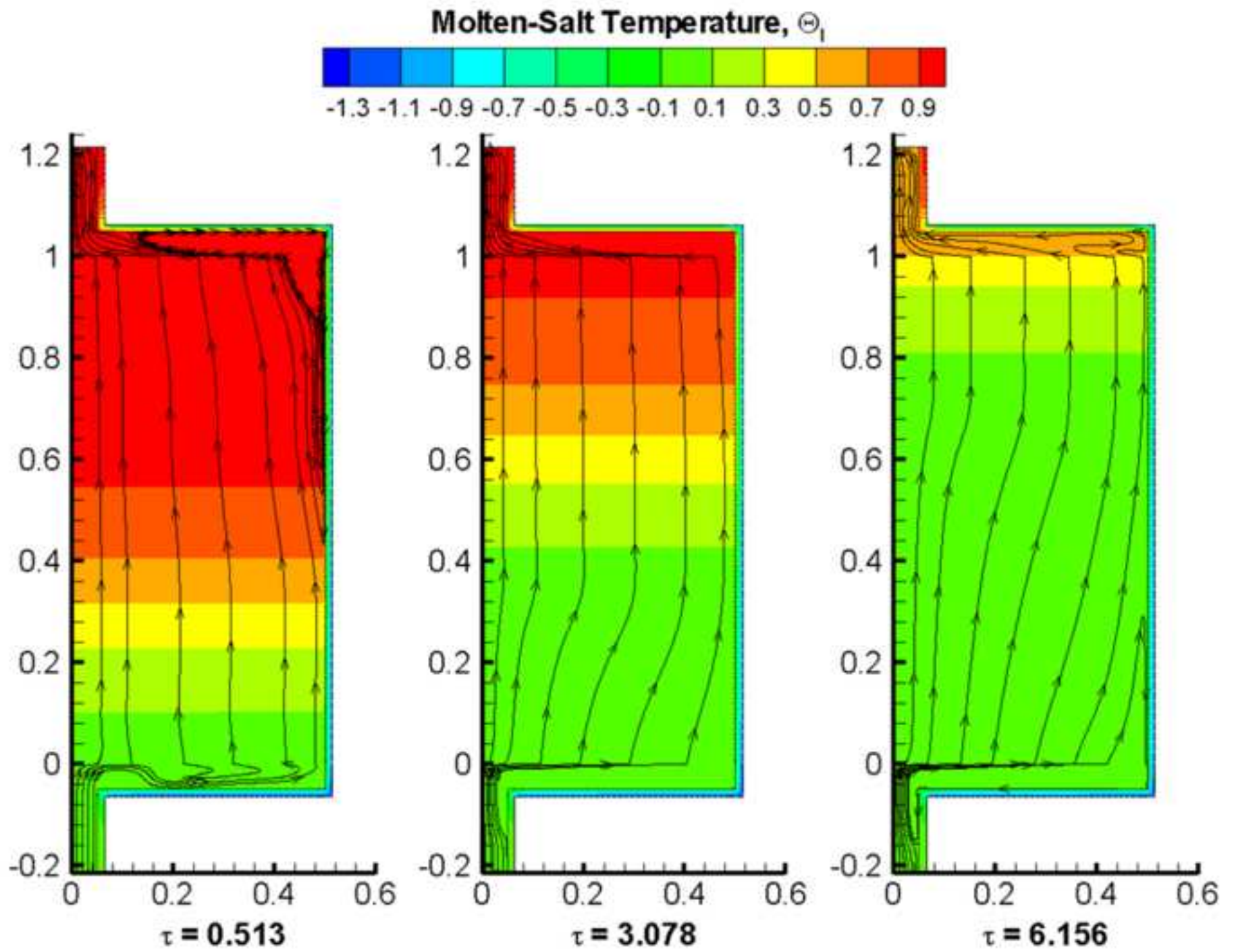


Figure_3

[Click here to download high resolution image](#)

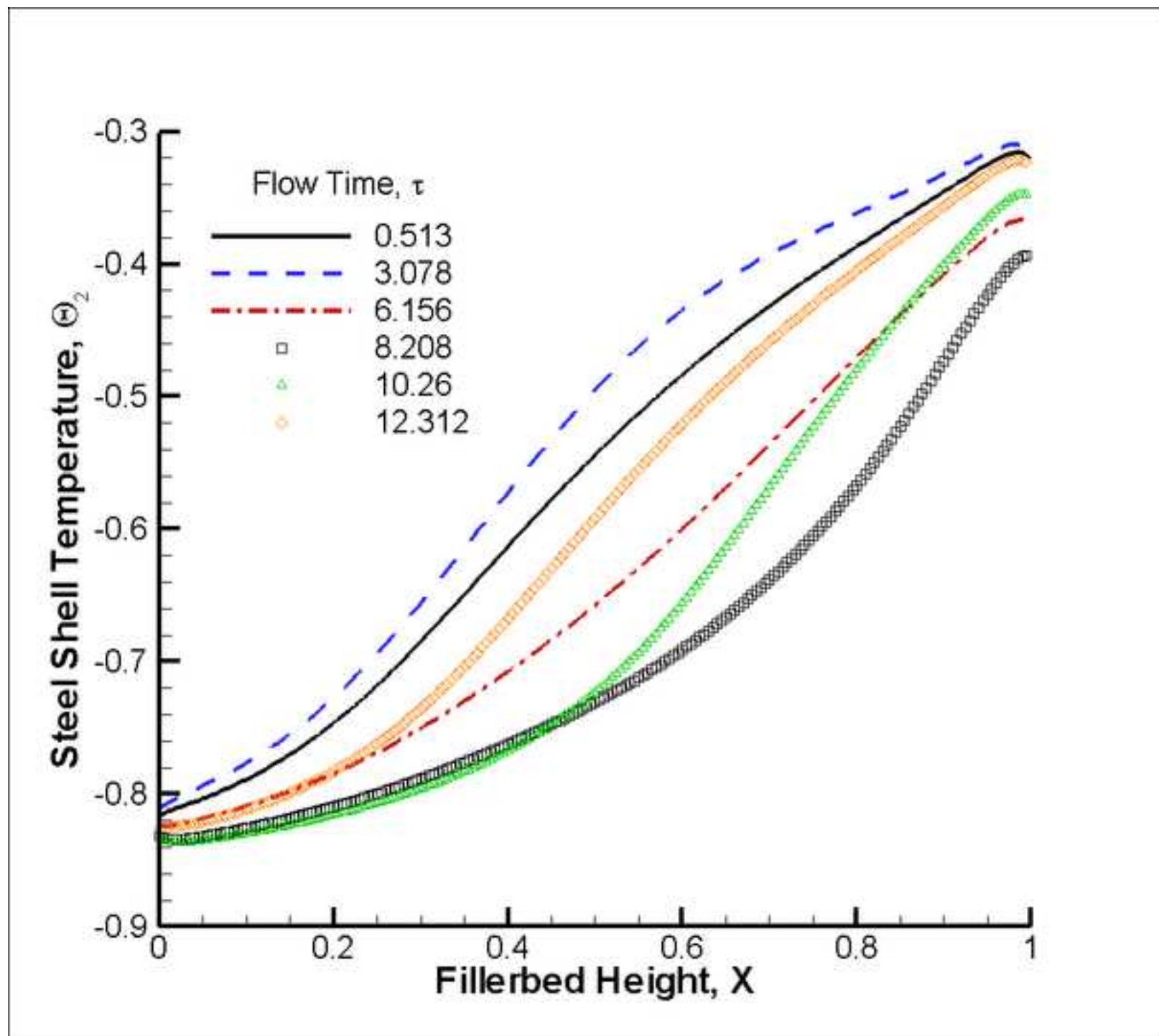


Figure_4

[Click here to download high resolution image](#)

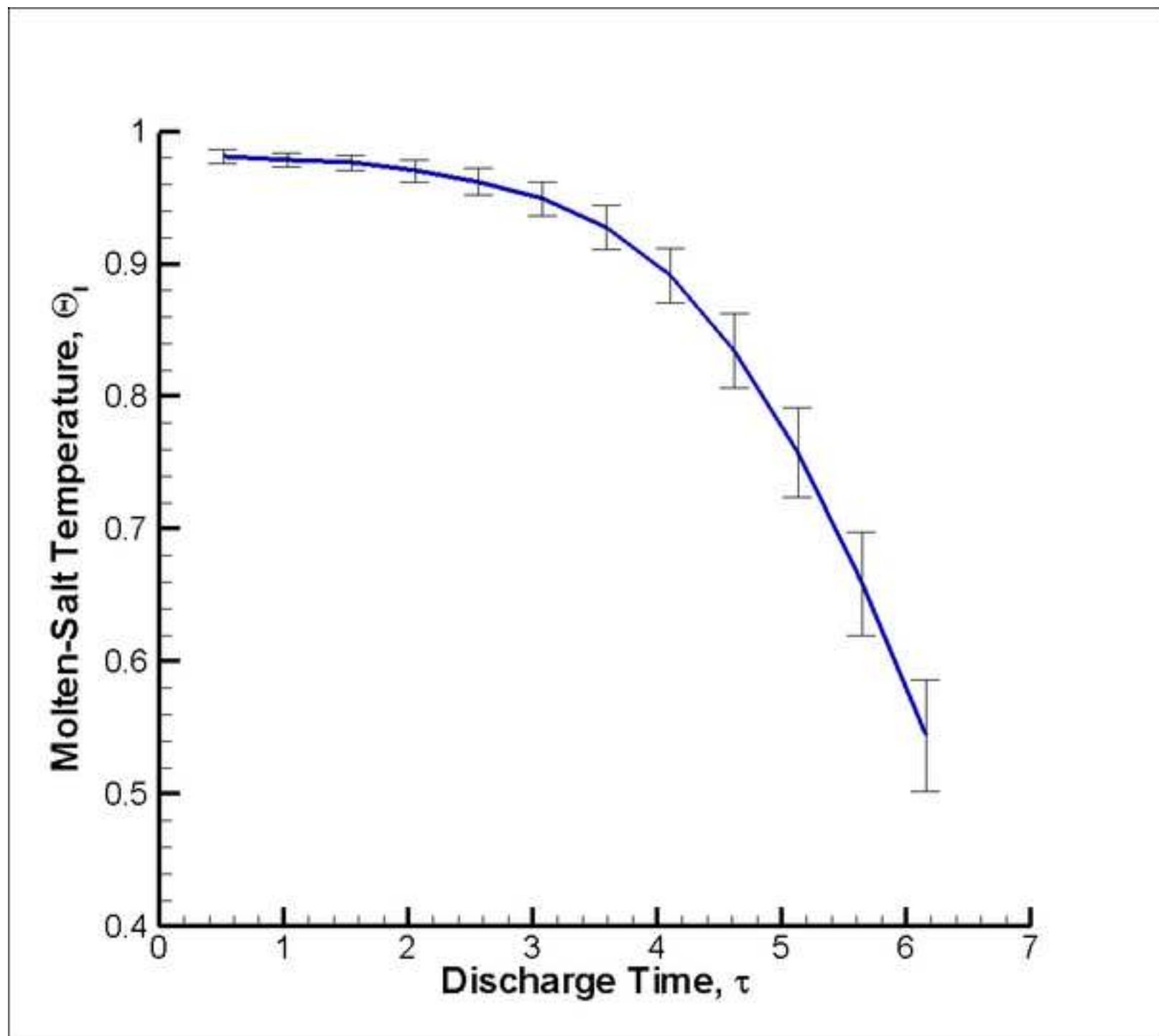


Figure_5

[Click here to download high resolution image](#)

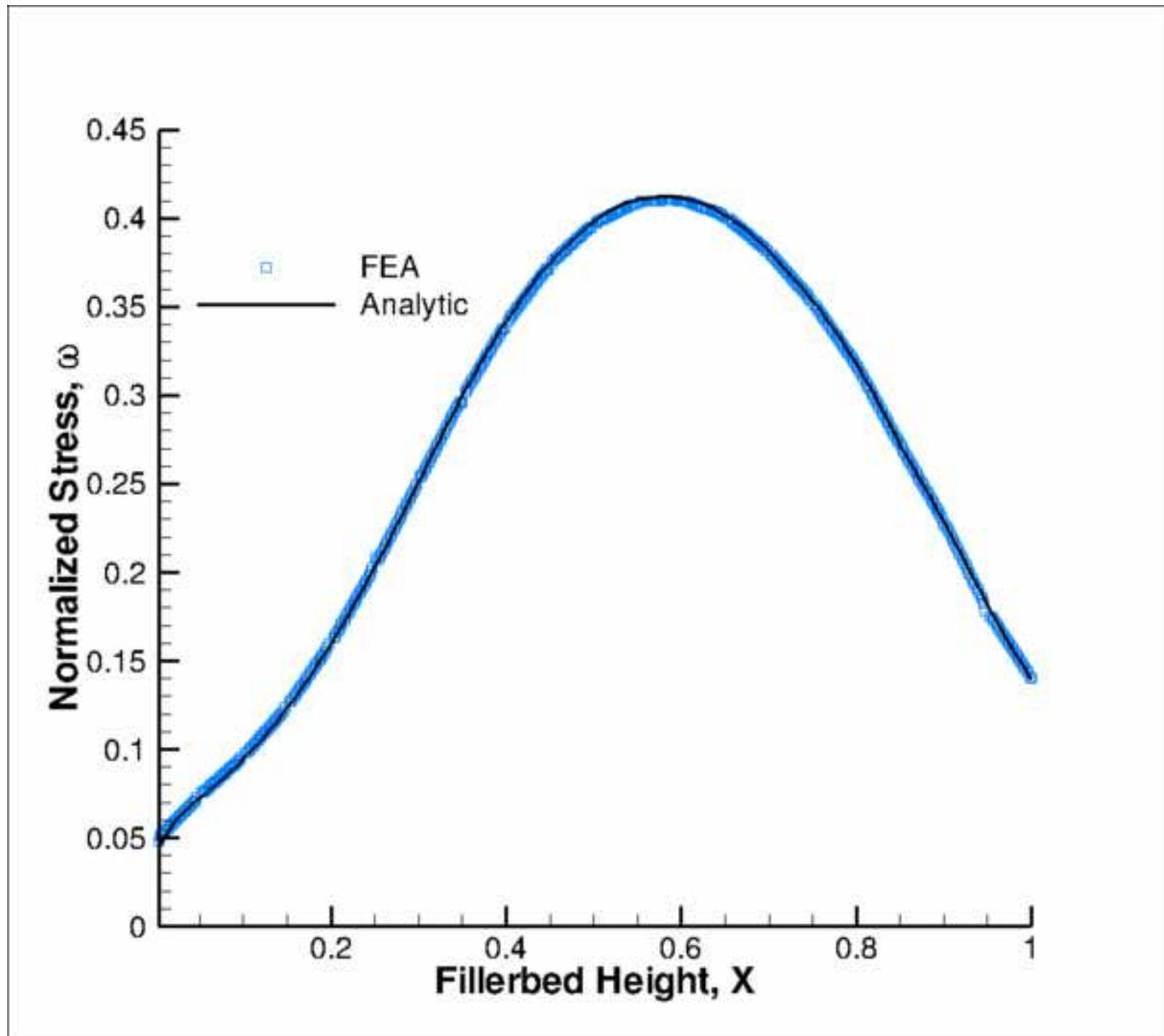
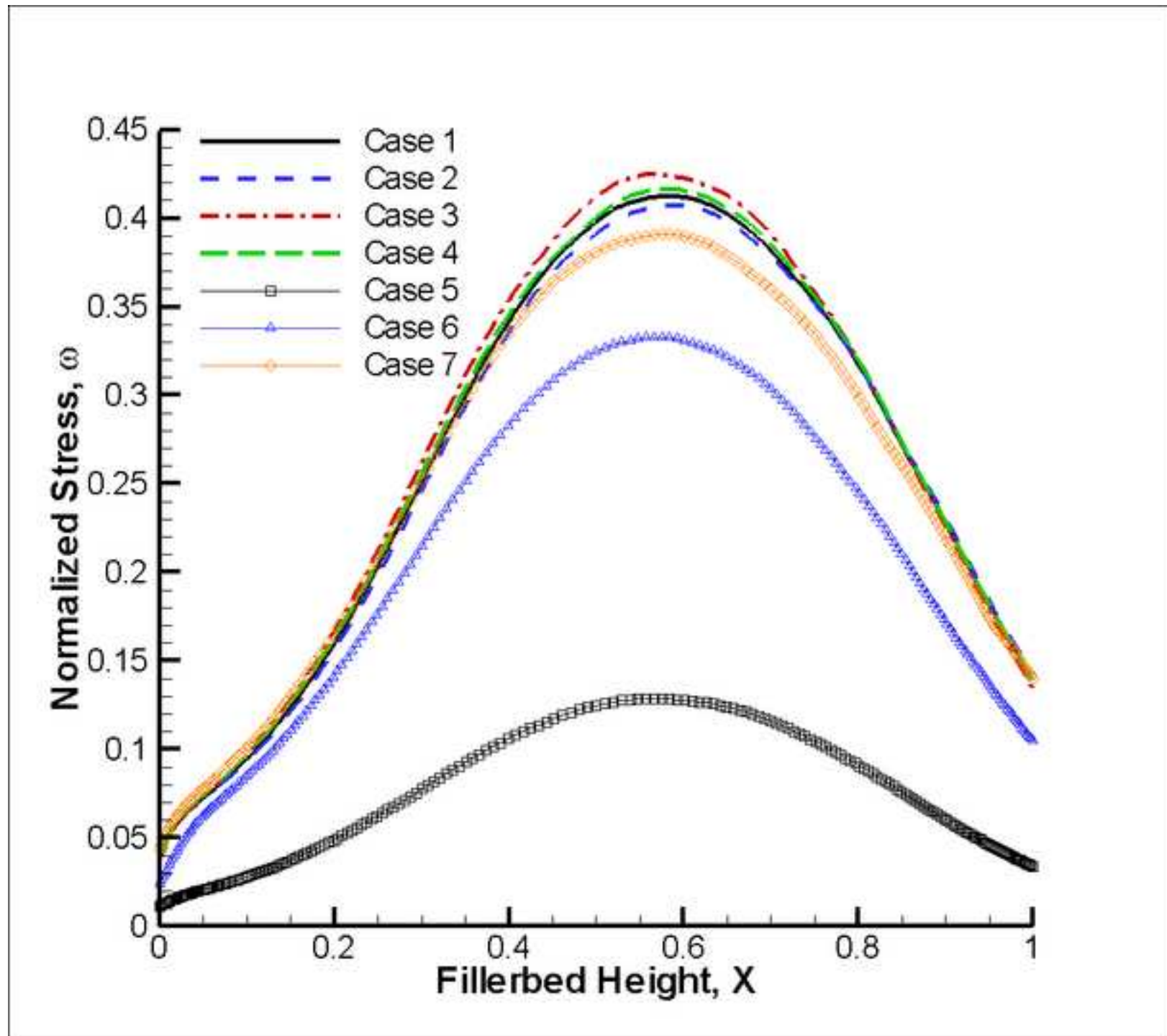


Figure_6

[Click here to download high resolution image](#)



Paper No. APEN-D-10-00807, "An Integrated Thermal and Mechanical Investigation of Molten-Salt Thermocline Energy Storage Applied Energy," Flueckiger, Yang and Garimella

Responses to Reviewers' Comments

The reviewers' comments are reproduced verbatim in italics, followed by the authors' responses.

Reviewer #1:

Thermal ratcheting in thermocline storage tanks is a timely solar-energy research topic and I applaud the authors attempt to contribute to the technical discussion of this issue. However, there are 2 major flaws in the work that need to be resolved before publishing.

- 1. The authors propose using a tank design that was actually built and tested at Sandia in the 1980s. There is no mention of the previous test that was performed, without the addition of the sand/gravel filler. The authors claim that this complex wall consisting of 3 layers can solve the problem. This reviewer doubts this will be true. First of all, the wall was actually 4 layers; the 4th layer is the waffle liner that keeps the salt away from the brick, as shown in reference 18. Furthermore, thermal ratcheting might result in excessive pressure on the fire brick causing them to be crushed between the liner and the shell. Yet, it is stated in the paper that "strain interactions with the firebrick ... is neglected." Rather than modeling this internally insulated tank, I suggest they model the largest thermocline ever built, the one tested at Solar One.*

We thank the reviewer's complementary remarks about the timeliness of this work.

In the revised manuscript, the literature review in the paper has been extended to include the composite wall tank mentioned by the reviewer (SAND87-3002). The corrugated liner material to prevent salt diffusion through the firebrick has also been included in the discussion to clarify the tank design, as seen in lines 11-19 page 4.

While internal insulation has been investigated before, past work has focused on two-tank storage systems without internal filler material. In this case, the amplitude of temperature oscillation in either the hot or the cold tank is significantly less and thermal ratcheting is not a relevant design issue. As such, internal insulation may not be as practical as external insulation to limit heat losses. In a thermocline storage system, the simultaneous containment of hot and cold fluid leads to large temperature changes and the potential for thermal ratcheting. From a heat transfer perspective, internal insulation is essential to limit heat losses but also to dampen the influence on the tank wall of the molten salt behavior.

In the present work, the main focus is on an analysis of the stresses in the steel tank wall. The mechanical performance of the firebrick (internal stress in individual bricks, etc.) depends on many undetermined factors, such as the manufacturing process and mounting details. An inclusion and discussion of these aspects is beyond the scope of a generalized analysis such as that in the present work. We also note that the term “firebrick” is used in a general sense to indicate the insulating layer inside the tank, and does not refer to a specific material. The revised manuscript shows the changes made in lines 15-18 page 10.

There may have been some confusion on one other point which the authors would like to clarify. The statement that “Strain interaction with the firebrick and ceramic sections is **neglected** as these layers are composed of loosely connected blocks, and are therefore unable to provide structural support to the filler region” was meant to indicate that the firebrick and ceramic layers do not provide any support to the filler bed. We did not imply that the internal stress of individual firebricks/ceramic blocks is negligible; however, a consideration of specific materials and their internal stresses was not the thrust of this work.

The authors do thank the reviewer for the suggestions regarding the stress in the firebrick material, and will attempt to include these practical considerations in future work. The current manuscript provides a clear description of a solution approach for thermal ratcheting issues. It should provide a good foundation for future comprehensive analyses from thermal, mechanical, material, and cost perspectives.

- 2. As stated in the paper, the structural analysis could not be validated due to absence of published data ... This is not entirely true since strain data was collected and structural analyses were performed prior to and during the test of the Solar One thermocline tank. The authors mention one of the Solar One reports (Reference 14), but only in passing. If the authors explore ref 14, they will find data and also see that a detailed structure analysis was performed in 1977, i.e. see ref 4 that is cited within ref 14. To validate their structural model, Purdue should model the Solar One thermocline tank and perform a detailed comparison of predictions from the Purdue structural model vs. the Solar One models/data. For example, for the tank temperature profiles found in Fig 11 and 12 of Ref 14, would Purdue's models predict the same hoop stress vs. height? Besides giving credence to the Purdue model, this comparison may discover new thinking on how to perform a structural analysis of a thermocline, including ratcheting. Does Purdue's independent analysis agree with the conclusions in the Solar One reports that ratcheting should not be a problem? The authors did a good job of validating their thermal model with experimental data in a previous paper (Ref 16 but incorrectly titled "Comprehensive analysis ...", the actual title was "Thermal analysis They need to do the same with their structural model as suggested above. At the same time, they could continue to validate their thermal model with thermal charge/discharge and cooldown data from Solar One, see McDonnell Douglas report cited in Ref 6.*

The goal of the present work was to present a first-of-its-kind analysis approach for thermal ratcheting and to use this approach to investigate means for mitigation of ratcheting from a thermal perspective. Central to this were the effects of added thermal resistances and various surface conditions on wall behavior, as discussed.

The authors agree that the Solar One thermocline was a historic achievement in thermal storage. There are some elements of the experimental data in Ref 14 that make a direct comparison to the present work difficult:

1. Thermal ratcheting was determined not to be a failure mode in the Solar One thermocline due to the greater thermal expansion of the filler relative to the tank wall.
2. The recorded data from the strain gages on the thermocline wall featured large experimental uncertainties.
3. The sporadic nature of the thermocline operation with Solar One prevents the verification of periodic operating conditions associated with the approach presented in the current manuscript.

As such, the authors believe that simulating the Solar One thermocline (while valuable for understanding the historic design) would not provide greater insight into the data or conclusions already presented in the paper. As stated before, we can consider a simulation of the Solar One tank in ongoing work.

The authors regret the error in the title of the paper in Ref 16 and have corrected the citation in the revised manuscript.

Reviewer #2:

1-Extrapolation of the concept to higher design temperatures such as 560C typical of Direct Central Receiver solar plants and up to 650C feasible if oxygen is used as cover gas in the storage tanks would be of much interest.

The use of higher temperatures would increase thermal oscillations associated with thermal ratcheting. However, the design approach discussed in the paper readily submits to scaling to these conditions.

2-Fire brick internal insulation hot salt through-leaks impact on the thermal and wall stress calculations and potential salt convective currents through the gap between fire brick layer and tank wall may be an issue in practical applications not considered in this article.

A thin liner material is present between the dual media and the internal insulation to prevent exposure to molten salt. The text has been amended to clarify this design point, as found in lines 21-23 page 6.

Reviewer #4:

Concentrated Solar Thermal (CST) power plants have been identified as a promising renewable option for the economical generation of electricity at a large scale. The use of a molten-salt thermocline for thermal energy storage (TES) in a CST power plant is believed to lead to a potential reduction in capital cost of 35% relative to a two-tank counterpart . In a molten-salt thermocline(large temperature gradient), a molten salt is used as the heat transfer fluid (HTF) that transports thermal energy between the storage unit and the other sections of the power system such as the collector field and the steam generator. Thermal ratcheting is a critical phenomenon associated with the cyclic operation of dualmedium thermocline tanks (hot and cold tank) in solar energy applications. Low-cost filler material quartzite rock is used to fill much of the volume in the thermocline tank. Thermoclines of this type are termed dual-media or multi-media storage systems. A comprehensive model of a thermocline tank that includes both the heterogeneous filler region as well as the composite tank wall is formulated and tested. The model accounts separately for the rock bed and interstitial molten salt regions in view of their different thermal properties. In this case the flowing resistance, pumping need to be considered, and the porous structure is not well-proportioned.

We thank the reviewer for the positive comments. Regarding the question raised, external pumping power must certainly be supplied to maintain fluid flow in the thermocline. However, a detailed analysis of the pumps is outside the scope of this paper. While the intent of the question about proportioning of the porous structure is not clear to the authors, it is noted that the difference in scale between the rock and size of the tank was previously investigated with detailed non-dimensional analysis in Ref 16.